2013 SCEC Annual Report

Forward modeling of fault slip rates, stress orientations, and distributed deformation in southern California with deformable microplate models

Principal Investigator:
Brendan Meade
Associate Professor
Harvard University
Department of Earth & Planetary Sciences
20 Oxford St.
Cambridge, MA 02138
meade@fas.harvard.edu
(617) 495-8921

Abstract

The San Andreas fault (SAF) marks the primary transform boundary between the Pacific and North American plates and has been studied intensively to determine the recurrence intervals of large earthquakes. Dense geologic and geodetic sampling along the SAF has revealed substantial variability in the along strike slip rate, with maxima approaching 40 mm/yr to the north and south of Los Angeles. In contrast, the San Bernardino segment of the SAF appears to slip at only 5–13 mm/yr, representing just 13–33% of the maximum SAF slip rate. Here we suggest that this spatial variation in slip rate may be explained by the interactions of deformable microplates driven by a combination of far-field plate motion boundary conditions and localized slip beneath the SAF. We find that the observed slip rate variations may be best described by models with 75% of Pacific-North America plate motion localized as slip beneath the SAF and 25% applied at the edges of the deforming plate boundary zone region. These models provide a mechanical explanation for why slip rates vary so significantly along the SAF and suggest a hybrid view of crustal deformation in southern California in which relative plate motion is accommodated by a combination of both localized and distributed deformation.

Technical report

This was a successful year of research and we accomplished all that we set out to do in our actual proposal! What follows is summary of the results of the deformable microplate modeling. This work has not been submitted for publication yet due to the fact that the student (Meredith Langstaff) has focused on writing up a much longer version of this for her Ph. D. dissertation defense, which is scheduled to occur this spring.

This intellectual merit of this work is to understand the behavior of models that integrate both on and "off"-fault deformation free of any kinematic constraints but subject to a simplified but geologically motivated representation of the fault system geometry in southern California. This approach is two-dimensional and neglects earthquake cycle processes precluding a direct comparison with interseismic geodetic observations. The merit of this is that we have explored and understand that behavior of this type of system for a wide range of boundary conditions including those that do not explain geologic slip data well (e.g., >30% "off" fault deformation).

The broader impact of this work is less immediately clear. The on-fault vs. "off"-fault debate is perhaps not as well posed as we might hope. To our knowledge all earthquakes occur on faults or initiate localized fracture. Thus in terms of implications for seismic hazard the "off"-fault component of deformation may not have a significant meaning other than 'off of faults that we commonly consider' and thus suggest regions where greater mapping may be of use. Alternatively if "off" fault were taken as a physical metric of strain that would never be released by earthquakes then it would require a rethinking of the ideas of moment balance and

the observation that geodetic and geologic slip rate budgets largely (though not entirely) agree across southern California. These comments are probably the biggest conclusions that we've arrived at through this work.

Deformable microplate models are based on a two-dimensional, elastic, two-step finite element approach. In these models, elastic deformation accrues within microplate interiors and discrete slip occurs at microplate boundaries (faults). For the purposes of the models described below, all faults are assumed to be frictionless. Initially, microplate boundaries are defined and microplates are individually meshed. Next, a global mesh is constructed that encompasses the entire model domain. In the first finite element step, displacement boundary conditions are applied to the global mesh. Advected microplate boundaries (faults) are interpolated from the resulting global displacement field. In the second finite element step, individual finite element solutions are calculated for each microplate using the advected boundaries as displacement boundary conditions. In this way we maintain geometric compliance and prevent unrealistic gaps and overlaps of tectonic microplates. Given the two-dimensional nature of these models, all faults represented are purely strike-slip. Deformable microplate modeling is more fully discussed in Chapter One of this text and in Langstaff and Meade (2013). Microplate boundaries in southern California are based on the locations of major mapped faults from the Southern California Earthquake Center Community Fault Model (Plesch et al., 2007). Together, this fault network forms 19 microplates constituting an idealized representation of the Pacific-North America plate boundary in southern California.

The microplates used for the deformable models presented here range in size from 4,000 km^2 to 200,000 km^2, with a maximum block edge length of 1000 km (the North America block). In all models, the eastern boundary of the North America block is subject to a zero-displacement boundary condition, approximating the nominally stable North American continent. In addition to the North America boundary condition, we explore a series of boundary conditions motivated by two previous modeling approaches used to explain the driving mechanisms at transform plate boundary zones. In the first, continental transform tectonics is treated as a broad region of distributed shear subject to mantle tractions or far-field displacement conditions (e.g., Lamb, 1994a; 1994b). The second approach draws from the suggestion of deeply routed and spatially constrained slip zones beneath major strike-slip faults (e.g. Corsini et al., 1991; Pili et al., 1997; West and Hubbard, 1997) and 15–40 km wide zones of mantle shear beneath such structures (e.g. Thatcher and England, 1998; Herquel et al., 1999; Moore et al., 2002; Rumpker et al., 2003) (though some authors have suggested shear zones of >100 km; Baldock and Stern, 2005) to suggest that transform motion occurs within localized lithospheric shear zones beneath large-scale strike slip faults such as the SAF (Platt et al., 2008; Platt and Becker, 2010). To test the relative contribution of each mechanism in producing observed slip rates on major southern

California faults, we develop a suite of deformable microplate models for the region. Distributed deformation end-member models are subject to 50 mm/yr displacement boundary conditions on the western edge of the model domain, consistent with relative plate motion estimates from DeMets et al. (1990). Because of the assumed elastic rheology, in the absence of faulting these models predict smoothly varying displacement rates across the plate boundary zone. In contrast, localized lithospheric shear zone models apply all 50 mm/yr of relative plate motion as slip beneath the SAF . In the context of the models presented here, this condition is implemented as an applied dis- placement along the SAF before geometric compliance is enforced. We also consider hybrid models, in which localized slip beneath the SAF increases incrementally, to find the combination of distributed deformation and localized deep slip that best match southern California slip rate estimates.

Model goodness-of-fit is assessed by comparing model-predicted SAF slip rates with along-strike geologic and geodetic slip rate estimates using the weighted sum of squared residuals. Residuals are calculated as the difference between the geologic or geodetic estimate and the model-predicted slip rate from the same location along strike. Residuals are then weighted by the error or spread associated with each observation and squared. End-member models that are purely edge driven (0 mm/yr slip beneath the SAF) and those where all displacements conditions are confined to the SAF (50 mm/yr slip beneath the SAF) have high WSSR values, suggesting neither give SAF slip rate predictions that are a good fit to geologic and geodetic estimates. Entirely edge driven models have WSSR values >350, and SAF slip rate predictions are consistently below geologic and geodetic estimates (Figure 1). Models where deformation is entirely driven by localized slip beneath the SAF have WSSR values >100 and over predict SAF slip rates (Figure 1). Notably, even in end-member models that localize all deformation on the SAF, slip rates along the central portion of the fault (e.g. the Mojave and San Bernardino segments) are <50 mm/yr, suggesting that the complex fault network in these regions plays a crucial role in partitioning deformation. In these regions, the SAF slips slower than the deep slip rate because of the curvilinear nature of the fault: here, SAF-bounding microplates must deform to satisfy the geometric compliance constraint and the equilibrium equations. These results suggest that a hybrid distributed deformation localized slip model is required to explain the SAF slip rate in the context of the particular modeling technique applied here.

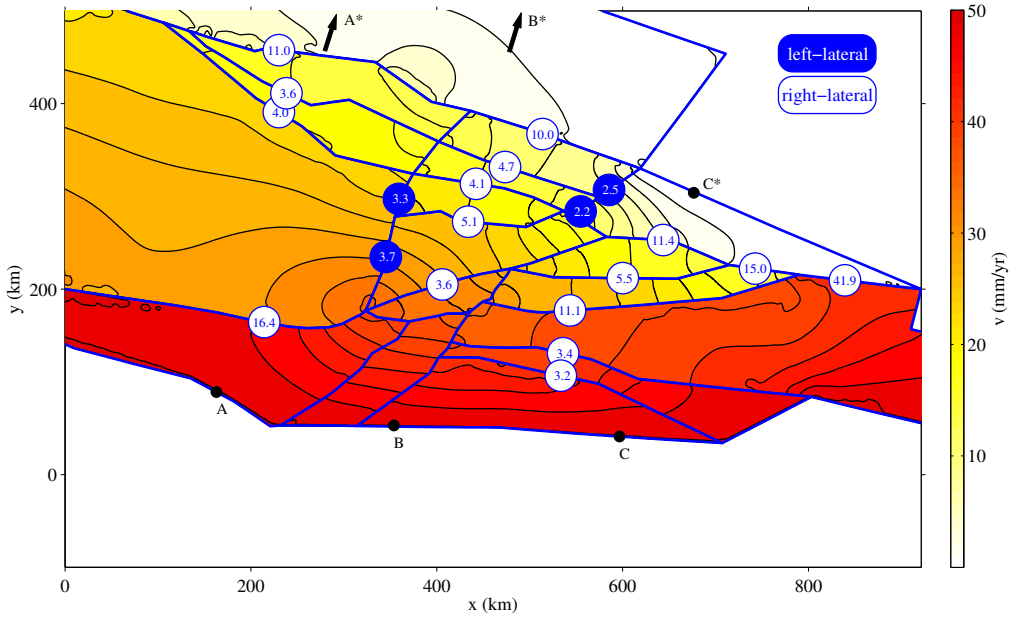

Figure 1. Slip rates and velocities from the distributed deformation end-member model. Microplate boundaries are shown as blue lines. Points A, A*, B, B*, C, and C* indicate end points for velocity profiles shown in Figure 2. Right-lateral slip rates are shown as white circles with blue text and left-lateral slip rates as blue circles with white text. For clarity, only representative slip rates are shown. Color shading shows velocity magnitudes, where redder colors indicate faster velocities. Maximum velocities equal the total relative motion between the Pacific and North American plates.

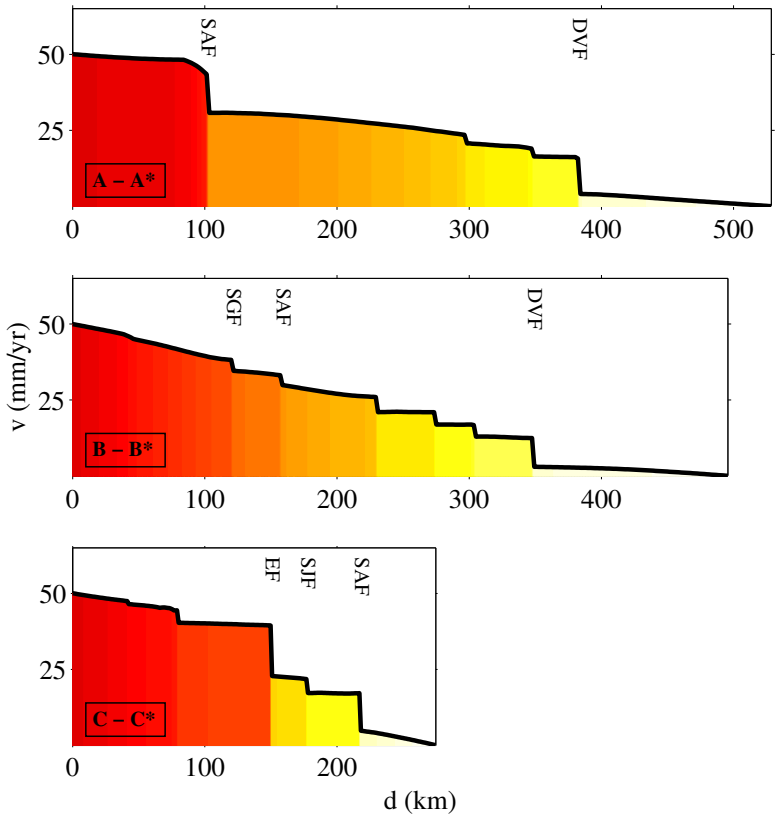

Figure 2. Velocity profiles across the northern (A-A*), central (B-B*), and southern (C-C*) extent of the distributed deformation end-member model. Profile end points are indicated in Figure 1. Color shading indicates velocity magnitudes and corresponds to velocity shading in Figure 1. Redder colors indicate faster velocities, with maximum velocities equal to the relative motion between the Pacific and North American plates. Here deformation decreases uniformly from west to east within microplates, though small discontinuities are evident at microplate boundaries (faults). In profile A offsets are the largest at the SAF, but offsets at the Death Valley fault and Elsinore fault are larger in profile B and profile C, respectively. SAF: San Andreas; DVF: Death Valley Fault; SGF: San Gabriel Fault; EF: Elsinore Fault; SJF: San Jacinto Fault.

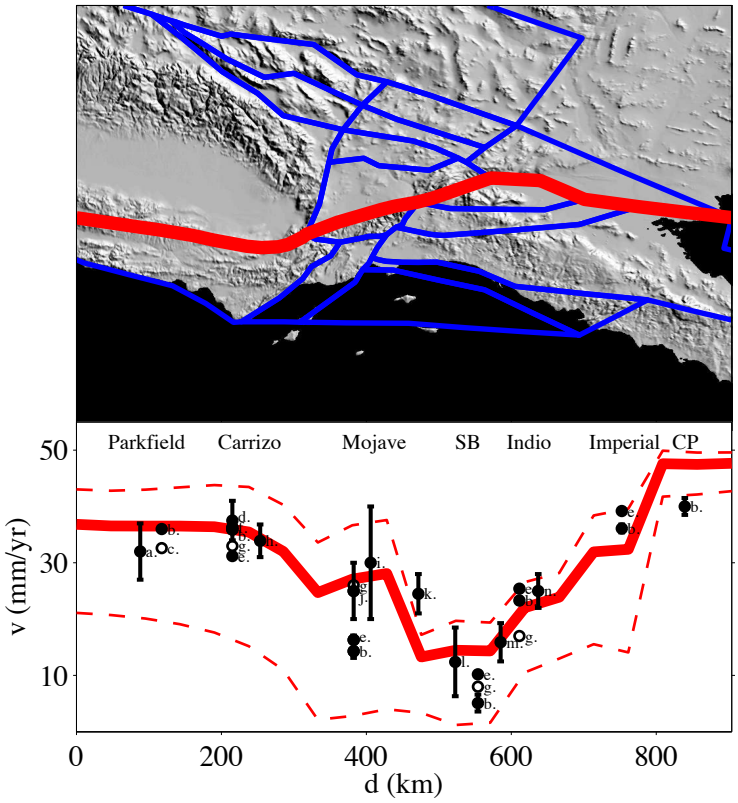

Figure 3. Predicted along strike slip rate for the San Andreas fault in southern California. The upper panel shows the rotated fault trace (red) and model mi- croplate boundaries (blue). Topography within 300 km of the SAF is shaded in gray. Model- predicted slip rates are shown in the lower panel with fault segment names indicated at the top (SB - San Bernardino and CP - Cerro Prieto). The bold red line indicates our best-fit hybrid model slip rate predictions, with ~36 mm/yr localized as deep slip beneath the SAF and ~14 mm/yr of distributed deformation applied on the western boundary of the model domain. End member models of purely distributed deformation (bottom dotted line) and entirely localized deep slip beneath the SAF (top dotted line) are also shown. Geologic and geodetic fault slip rate estimates are shown as black circles with reported 1-sigma error bars r as white circles when estimate error is not reported. Both observations and model predictions have maxima on the northern and southern segments of the model domain and both reach a minimum on the San Bernardino segment. Slip rates inferred from geologic and geodetic data are taken from: a. Savage and Burford, 1973; b. Meade and Hager, 2005; c. Murray et al., 2001; d. Segall, 2002; e. Loveless and Meade, 2011; f. Schmalzle et al., 2006; g. Chuang and Johnson, 2011; h. Sieh and Jahns, 1984; i. Matmon et al., 2005; j. McCaffrey, 2005; k. Weldon and Sieh, 1985; l. McGill et al., 2013; m. Van der Woerd, 2006; n. Fialko et al., 2006.

References

Baldock, G., and Stern, T., 2005, Width of mantle deformation across a continental transform: Evidence from upper mantle (Pn) seismic anisotropy measurements, Geology, v. 33, n. 9, p. 741-744, doi: 10.1130/G21605.1.

Becker, T. W., Hardebeck, J. J., and Anderson, G., 2005, Constraints on fault slip rates of the southern California plate boundary from GPS velocity and stress inversions, Geophysical Journal International, v. 160, p. 634-650.

Bennett, R. A., Rodi, W., and Reilinger, R. E., 1996, Global Positioning System constraints on fault slip rates in southern California and northern Baja, Mexico, Journal of Geophysical Research, v. 101, n. B10, p. 21,943-21,960.

Bird, P., and Rosenstock, R.W., 1984, Kinematics of present crust and mantle flow in southern California, Geological Society of America Bulletin, v. 95, p. 946-957.

Bird, P., Kong, X., 1994, Computer simulations of California tectonics confirm very low strengths of major faults, Geological Society of America Bulletin, v. 106, p. 159-174.

Bourne, S. J., England, P. C., and Parsons, B., 1998, The motion of crustal blocks driven by flow of the lower lithosphere and implications for slip rates of continental strike-slip faults, Nature, v. 391, p. 655-659.

Cheng, A., Jackson, D. D., and Mitsuhiro, M., 1987, Aseismic crustal deformation in the Transverse Ranges of southern California, Tectonophysics, v. 144, p. 159-180.

Chuang, R. Y., and Johnson, K. M., 2011, Reconciling geologic and geodetic model fault slip-rate discrepancies in southern California: Consideration of nonsteady mantle flow and lower crustal fault creep, Geology, v. 39, no. 7, p. 627-630, doi: 10.1130/G32120.1.

Corsini, M., Vauchez, A., Archanjo, C., and de Sá, E. F. J., 1991, Strain transfer at continental scale from a transcurrent shear zone to a transpressional fold belt: The Patos-Seridó system, northeastern Brazil, Geology, v. 19, p. 586-589.

DeMets, C., Gordon, R. G., Argus, D. F., and Stein, S., 1990, Current plate motions: Geophysical Journal International, v. 101, p. 425-478.

DeMets, C., and Dixon, T. H., 1999, New kinematic models for Pacific-North America motion to present, I: Evidence for steady motion and biases in the NUVEL-1A model, Geophysical Research Letters, v. 26, no. 13, p. 1921-1924.

Ekström, G., and England, P., 1989, Seismic strain rates in regions of distributed continental deformation, Journal of Geophysical Research, v. 94, n. B8, p. 10,231-10,257.

Fialko, Y., 2006, Insterseismic strain accumulation and the earthquake potential on the southern San Andreas fault system, Nature, v. 44, p. 968-971.

Flesch, L. M., Holt, W. E., Haines, A. J., and Shen-Tu, B., 2000, Dynamics of the Pacific-North American plate boundary in the western United States, Science, v. 287, p. 834-836.

Herquel, G., Tapponnier, P., Wittlinger, G., Mei, J, and Danian, S., 1999, Teleseismic shear wave splitting across the Altyn Tagh fault, Geophysical Research Letters, v. 26, n. 21, p. 3225-3228.

Lamb, S. H., 1994, Behavior of the brittle crust in wide plate boundary zones, Journal of Geophysical Research, v. 99, n. B3, p. 4457-4483.

Lamb, S., 1994, A simple method for estimating the horizontal velocity field in wide zones of active deformation – I. Description, with an exampld from California, Geophysical Journal International, v. 119, p. 297-312.

Loveless, J. P., and Meade, B. J., 2011, Stress modulation on the San Andreas fault by interseismic fault system interactions, Geology, v. 39, no. 11, p. 1035-1038, doi: 10.1130/G32215.1.

Matmon, A., Schwartz, D. P., Finkel, R., Clemmens, S., and Hanks, T., 2005, Dating offset along the Mojave section of the San Andreas fault using cosmogenic ^{26}Al and ^{10}Be, GSA Bulletin, v. 117, no. 5/6, p. 795-807, doi: 10.1130B25590.1.

McCaffrey, R., 2005, Block kinematics of the Pacific-North America plate boundary in the southwestern United States from inversion of GPS, seismological, and geologic data, Journal of Geophysical Research, v. 110, no. B07401, doi: 1029/2004JB003307.

McGill, S. F., Owen, L. A., Wheldon, R. J., and Kendrick, K. J., 2013, Latest Pleistocene and Holocene slip rate for the San Bernardino strand of the San Andreas fault, Plunge Creek, Southern California: Implications for strain partitioning within the southern San Andreas fault system for the last ~35 k.y., GSA Bulletin, doi: 10.1130/B30647.

Meade, B. J., and Hager, B. H., 2005, Block models of crustal motion in southern California constrainted by GPS measurements, Journal of Geophysical Research, v. 110, no. B03403, doi: 10.1029/2004JB003209.

Moore, M., England, P., and Parsons, B., 2002, Relation between surface velocity field and shear wave splitting in the South Island of New Zealand, Journal of Geophysical Research, v. 107, n. B9, doi: 10.1029/2000JB000093.

Murray, J. R., Segall, P., Cervelli, P., Prescott, W., and Svarc, J., 2001, Inversion of GPS data for spatially variable slip-rate on the San Andreas fault near Parkfield, CA, Geophysical Research Letters, v. 28, no. 2, p. 359-362.

Pili, É., Ricard, Y., Lardeaux, J.-M., and Sheppard, S. M. F., 1997, Lithospheric shear zones and mantle-crust connections, Tectonophysics, v. 280, p. 15-29.

Platt, J. P., Kaus, B., and Becker, T. W., 2008, The mechanics of continental transforms: An alternative approach with applications to the San Andreas fault system and the tectonics of

California, Earth and Planetary Science Letters, v. 274, p. 380-391, doi: 10.1016/j.epsl.2008.07.052.

Platt, J. P., and Becker, T. W., 2010, Where is the real transform boundary in California?, Geochemistry, Geophysics, Geosystems, v. 11, n. 6., doi: 10.1029/2010GC003060.

Plesch, A., Shaw, J. H., Benson, C., Bryant, W. A., Carena, S., Cooke, M., Dolan, J., Fuis, G., Gath, E., Grant, L., Hauksson, E., Jordan, T., Kamerling, M., Legg, M., Lindvall, S., Magistrale, H., Nicholson, C., Niemi, N., Oskin, M., Perry, S., Planansky, G., Rockwell, T., Shearer, P., Sorlien, C., Süss, P. M., Suppe, J., Treiman, J., and Yeats, R., 2007, Community fault model (CFM) for southern California, Bulletin of the Seismological Society of America, v. 97, n. 6, p. 1793-1802, doi: 10.1785/0120050211.

Rümpker, G., Ryberg, T., Bock, G., and Desert Seismology Group, 2003, Boundary layer mantle flow under the Dead Sea transform fault inferred from seismic anisotropy, Nature, v. 425, p. 497-501.

Savage, J. C., and Burford, R. O., 1973, Geodetic determination of relative plate motion in central California, Journal of Geophysical Research, v. 78, no. 5, p. 832-845.

Schmalzle, G., Dixon, T., Malservisi, R., and Govers, R., 2006, Strain accumulation across the Carrizo segment of the San Andreas fault, California: Impact of laterally varying crustal properties, Journal of Geophysical Research, v. 111, no. B05403 doi: 10.1029/2005JB003843.

Segall, P., 2002, Integrating geologic and geodetic estimates of slip rate on the San Andreas fault system, International Geology Review, v. 44, p. 62-82.

Sieh, K. E., and Jahns, R. H., 1984, Holocene activity of the San Andreas fault at Wallace Creek, California, Geological Society of America Bulletin, v. 95, p. 883-896.

Thatcher, W., and England, P. C., 1998, Ductile shear zones beneath strike-slip faults: Implications for the thermomechanics of the San Andreas fault zone, Journal of Geophysical Research, v. 103, n. B1, p. 891-905.

Weldon, R. J., Fumal, T. E., Biasi, G. P., and Scharer, K. M., 2005, Past and future earthquakes on the San Andreas fault, v. 308, 966-967.

Weldon, R., and Humphreys, E., 1986, A kinematic model of southern California, Tectoncs, v. 5, no. 1, p. 33-48.

West, D. P., and Hubbard, M. S., 1997, Progressive localization of deformation during exhumation of a major strike-slip shear zone: Norumbega fault zone, south-central Maine, USA, Tectonophysics, v. 273, p. 185-201.